A multiple-beam sector antenna with a dual planar reflectarray arrangement

Michael Thiel and Wolfgang Menzel*
Microwave Techniques, University of Ulm, D-89069 Ulm, Germany
*Email: wolfgang.menzel@ieee.org

***Abstract*— A multiple-beam sector antenna realized with a dual planar reflectarray arrangement is presented. A 58 GHz antenna with three feeds was built up and tested. Antenna dimensions are 150 mm diameter and 40 mm height, and each feed covers distinct 30°-sectors in one plane in combination with a small beamwidth in the orthogonal plane.**

I. Introduction

Over the last years, the frequency band around 60 GHz has attracted more and more interest for wireless local area communication and networks [1]. This band allows high transmission rates and needs not to be licensed in many countries of the world. Additionally, the required components are small and lightweight and can nowadays be produced with low cost.

For such wireless networks with a cellular structure, standard sector antennas are required, since it is impossible to adapt the antennas to the individual situations. These standard antennas illuminate a sector of 30°, 60° and 90° in one plane and exhibit a narrow beam in the orthogonal plane.

In crowded places, only 30°-sector antennas can keep high transmission rates for the individual users in a cellular structure. But such a network structure is expensive in terms of the number of antennas and their adjustment. The antenna presented in this work provides a solution, it combines three standard 30°-sector antennas, illuminating 90° in total, in one low-cost dual planar reflectarray arrangement.

II. Basic principle of a dual planar reflectarray antenna

The basic cross section of a dual reflectarray antenna [2], [3] is sketched in figure 1. The setup is an enhancement of a folded reflector antenna [4], [5], which only differs from the dual reflectarray antenna in the upper reflector.

The radiation from the feed is polarized in such a way that it is reflected by the polarizing grid of the upper reflector. Additionally, narrow dipoles in the direction of the grid are printed on the lower side of the upper reflector which allow adjustments of the reflected wave's phase through their lengths. Then the wave is incident on the lower reflectarray with printed rectangular patches. The patch axes of this array are tilted by 45° with respect to the incident field. The electric field vector can be decomposed into the two components parallel to the patch axes, and the reflection properties can be determined separately. The dimensions of the patches are selected in such a way that a phase difference of 180° occurs between the reflection phase of these two components. Superposition of the reflected field components then leads to a twisting of the polarization by 90° (fig. 2). The necessary 180° reflection phase difference between the two field components of the reflected wave can be achieved for a large number of combinations of length and width of the patches differing by the absolute reflection phase.

In summary, this antenna structure provides two degrees of freedom to modify the wavefront of the feeding horn.

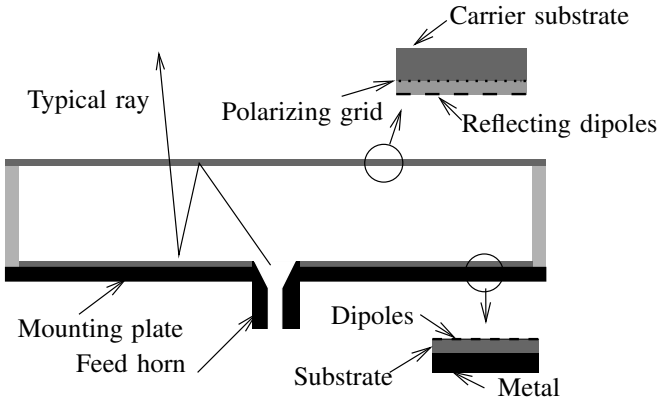

Fig. 1. Cross section of a dual reflectarray antenna.

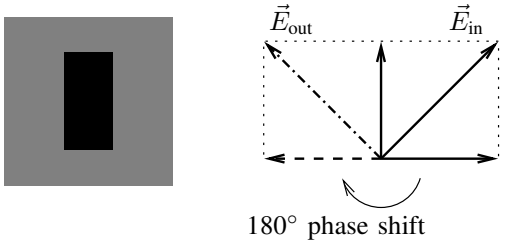

Fig. 2. Single cell with patch and vector decomposition of incident and reflected electric field for 180° of reflection phase angle difference.

III. Design of the Multiple Beam Sector Antenna

A. Calculation of the Amplitude and Phase Distribution for a Tilted Sector Beam

In order to derive the far-field pattern of the antenna, one needs to know the amplitude and phase distribution on the lower reflector. First, the mapping of the amplitude distribution on the upper reflector to the lower reflector has to be found.

Given the reflection phase of the upper reflector (described by the electrical length $\Phi_1(x, y)$), the mapping can be calculated with the law of reflection for frequency selective surfaces combined with the law of energy conservation. The law of reflection for a two-dimensional reflector was introduced in [3], it allows tracing of rays (fig. 3) from the feed position $(x_f, 0, z_f)$ over the reflection point at the upper reflector (x_1, y_1, d) down to the lower reflector $(x_2, y_2, 0)$. In this approach, it is assumed that the antenna reflectors are symmetric with respect to the x- and y-axis. The feeds all are placed on the x-axis, and z_f is the distance of the feed above the lower reflector. With the distance $l = \sqrt{(x_1 - x_f)^2 + {y_1}^2 + (d - z_f)^2}$ between the feed position and the reflection point at the upper reflector, the endpoint on the lower reflector $(x_2, y_2, 0)$ results in:

$$x_2(x_1, y_1) = x_1 + \frac{v(x_1, y_1) \cdot d}{\sqrt{1 - v(x_1, y_1)^2 - u(x_1, y_1)^2}}, \quad (1)$$

$$y_2(x_1, y_1) = y_1 + \frac{u(x_1, y_1) \cdot d}{\sqrt{1 - v(x_1, y_1)^2 - u(x_1, y_1)^2}}, \quad (2)$$

with

$$v(x_1, y_1) = \frac{\partial \Phi_1(x_1, y_1)}{\partial x} + \frac{x_1 - x_f}{l}, \quad (3)$$

$$u(x_1, y_1) = \frac{\partial \Phi_1(x_1, y_1)}{\partial y} + \frac{y_1}{l}. \quad (4)$$

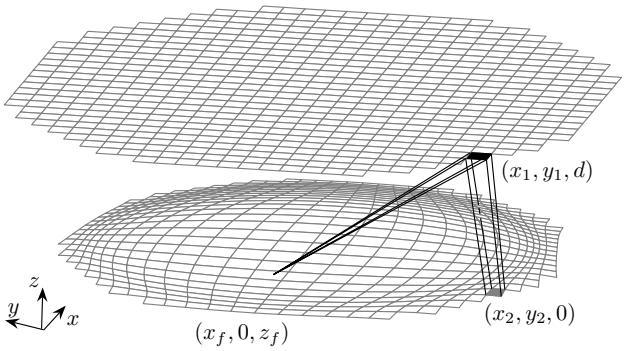

Fig. 3. Mapping of the upper reflector's grid to the lower reflector. The path of the rays for one blackened square of the upper reflector down to the lower reflector is shown.

The law of energy conservation connects the power densities on both reflectors [3]:

$$I_1 \cdot \mathrm{d}A_1 = I_2 \cdot \mathrm{d}A_2 . \quad (5)$$

The power density I_1 of a small square $\mathrm{d}A_1$ on the upper reflector multiplied by its area is equivalent to the respective power density I_2 on the lower reflector multiplied by the area mapped from the upper to the lower reflector. Now a small homogenous rectangular grid on the upper reflector can be mapped on the lower reflector (fig. 3) using equations (1) and (2). So for every small square $\mathrm{d}A_1$ on the upper reflector, the corresponding area $\mathrm{d}A_2$ on the lower reflector is known, and the power density on the lower reflector can be calculated.

The derivation of the phase distribution on the lower reflector also uses the ray-tracing equations (1) and (2): Given the path of the ray from the feed to the lower reflector, the phase on the lower reflector $\varphi(x_2, y_2)$ is the summation of the length of the path times the wavenumber $2\pi/\lambda_0$ and the reflection phases on both reflectors the ray intersects ($\varphi_1(x_1, y_1)$ and $\varphi_2(x_2, y_2)$):

$$\begin{aligned}\varphi(x_2, y_2) = & -\frac{2\pi}{\lambda_0} \cdot \Big(\sqrt{(x_1 - x_f)^2 + {y_1}^2 + (d - z_f)^2} + \\ & + \sqrt{(x_2 - x_1)^2 + (y_2 - y_1)^2 + d^2}\Big) + \\ & + \varphi_1(x_1, y_1) + \varphi_2(x_2, y_2) . \end{aligned} \quad (6)$$

B. Derivation of the Reflector Contours

The derivation of the reflector contours is based on the iterative 2D ray-tracing of a bifocal folded reflector antenna introduced in [2]: With the symmetry of the antenna, a given feed point for the side and the reflection angles of the outgoing rays from the lower reflector, a set of data can be found for both reflectors. The ray-tracing procedure is described in [2], here the only difference is that the reflection angles of the outgoing rays from the lower reflector go linearly from 15° to 45° in order to get a 30°-sector. The resulting set of data is approximated by two polynomials.

Going into 3D, the upper reflector is build up rotationally symmetrical out of the polynomial, and for the lower reflector the polynomial provides the phase distribution in one direction (along x-axis). Orthogonal to it, the phase of the outgoing wave has to be constant because a narrow beam in this plane is required. The reflector contours of the iterative 2D ray-tracing are the starting point for an optimization procedure since its far-field is unsatisfactory. For both central feed and feed on the side, the far-field in the plane of the sectors is calculated, compared to ideal 30°-sectors, and the difference is minimized.

The resulting phase distribution on the upper reflector after the 2D ray-tracing is shown in fig. 4. The phase decreases rapidly outwards to the edge of the reflector (at 70 mm), therefore the further outside a ray from the feed hits the upper reflector the more it is reflected back towards the feed. Because of this the upper reflector highly focusses the initial wave of the feed. The focussing is visualized in fig. 5. The path of the rays from the feed point to the lower reflector is plotted for both side and middle feed in the xz-plane. The rays of both feed points hit the lower reflector inside a circle with a radius of 60 mm. Now if one calculates the amplitude and phase distributions on the lower reflector, the phase distributions of both feeds nearly match after $2\pi/\lambda_0 \cdot x \cdot \sin 30°$ was subtracted from the phase distribution of the side feed (corresponds to a 30°-shift of the farfield). Furthermore, since there is an additional degree of freedom in the the tilt angle of the side feed, it can be choosen in a way that the amplitude distributions of both feed points nearly match, too.

Having this in mind, the starting point for the optimization procedure can be refined: The upper reflector of the 2D-ray-tracing was only used to calculate the amplitude distribution

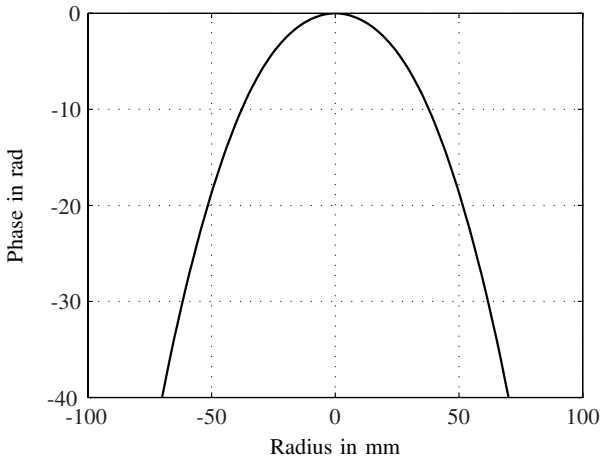

Fig. 4. The reflection phase distribution of the upper reflector.

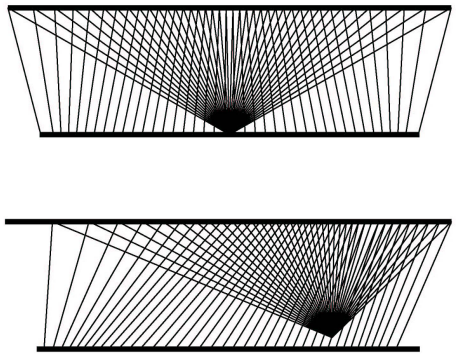

Fig. 5. Ray paths from the feed to the lower reflector in the xz-plane for both feed points.

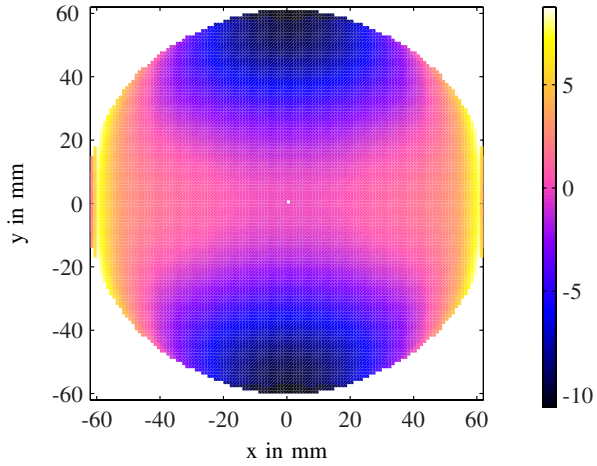

Fig. 6. The reflection phase distribution of the lower reflector in rad.

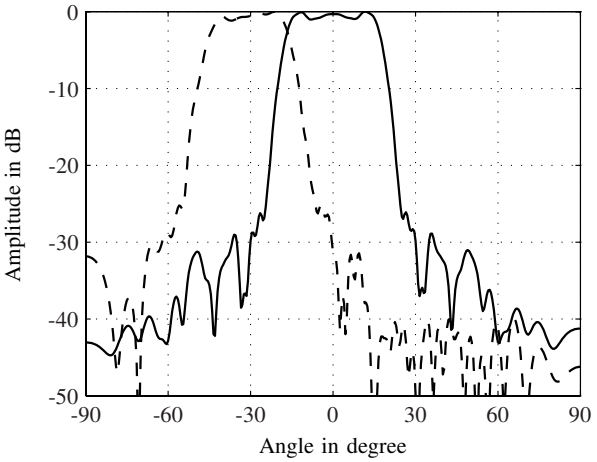

Fig. 7. The theoretical array factor in the sector plane for both feed points.

on the lower reflector. For this amplitude distribution, the required phase distribution leading to a 30°-sector was derived with phase synthesis according to the method of stationary phase [6]. The new lower reflector contour was then used as the starting point of the optimization. This lead to a more accurate far-field at the start of the optimization yielding less optimization time.

The reflection phase distribution on the lower reflector after optimization is plotted in fig. 6. Because of the focussing effect, the radius of the reflector is only 60 mm. The reflection phase increases a bit going outwards on the x-axis in order to shape the 30°-sector, and it decreases along the y-axis in order to compensate the increasing path length of the rays in this direction.

The theoretical array factor of the described reflector contours is plotted in fig. 7. Since the amplitude- and phase distribution for both feeds do not exactly match one can see a small ripple on both sectors and side lobes up to -30dB. This is the best tradeoff one can get if both sectors are optimized at the same time. An optimization of only one sector would lead to a better contour of the optimized sector but would worsen the non-optimized sector.

At last, the reflection phases for the two reflectors are transferred into the respective patch dimensions. The front substrate is realized as a double-layer structure to improve stability.

IV. Results and Measurements

An antenna has been designed, fabricated and tested. Figure 8 shows the photograph of the multiple-beam sector antenna with the upper substrate removed.

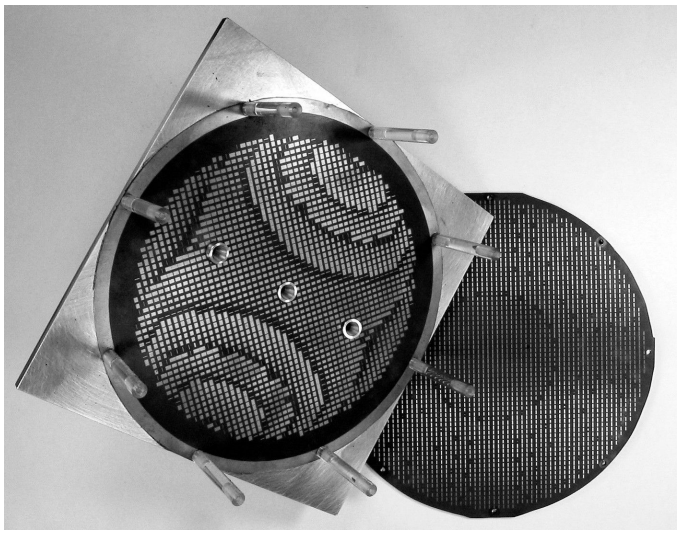

Fig. 8. Photograph of the fabricated folded dual reflectarray antenna.

The overall antenna diameter is 150 mm, and the distance between the two reflectors is 40 mm. Both substrates are 0.254 mm thick, the carrier substrate for the upper reflector is 1.41 mm thick. The dielectric constant of all layers is 2.2. The feeds are circular waveguide horns with a conus angle of 11.7° and a gain of 11 dB. The horn for the sectors on the side are placed 34.1 mm away from the center, 1 mm above the patch-plane and tilted 9.3° towards the center. Fig. 9 illustrates the H-plane characteristic of the complete antenna at 57.5 GHz for all feeds. Every feed point is associated to a 30°-sector, only the outer sectors are shifted a bit inward. The ripple of the outer sector diagram is less than ±1.8 dB, the ripple of middle sector less than ±1.0 dB. Fig. 10 shows the E-plane characteristic for both one feed on the side and the feed in the middle for two different cuts through the sectors at the shown angles. The beamwidth in the E-plane is always 3°, and the sidelobe level is better than -12.5 dB for the central beam and better than -16.0 dB for the side beam. A very similar performance is found over a bandwidth of 57.5 GHz ± 1 GHz.

V. Conclusion

A novel multiple beam sector antenna based on a double reflectarray arrangement has been presented. Therefore, the principle of a bifocal folded reflectarray antenna [2] was successfully extended with a calculation method for the amplitude and phase distribution inside the antenna in order to be able to derive sector patterns.

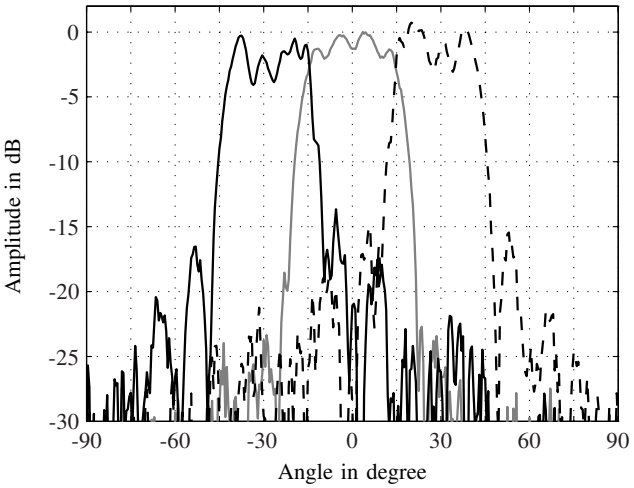

Fig. 9. H-plane radiation diagram of the antenna at 57.5 GHz with all feeds normalized on maximum of the center feed.

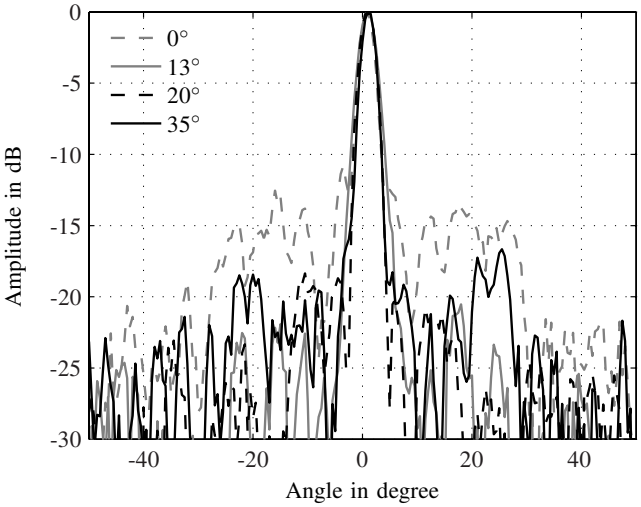

Fig. 10. Normalized E-plane radiation diagram for both center and side feed for different cuts through the sectors at 57.5 GHz.

References

[1] Y. Takimoto and T. Ihara, "Research activities on millimeter wave indoor communication systems in Japan," in *Microwace Symposium Digest Vol. 2*, 1993, pp. 673–676.

[2] W. Menzel, M. Al-Trikriti, and R. Leberer, "A 76 GHz multibeam planar reflector antenna," in *European Microwave Conference (EuMC '02)*, 2002, pp. 977–980.

[3] R. Leberer and W. Menzel, "A dual planar reflectarray with synthesized phase and amplitude distribution," *IEEE Transactions on Antennas and Propagation*, vol. 53, pp. 3534–3539, 2005.

[4] W. Menzel, D. Pilz, and R. Leberer, "A 77 GHz FM/CW radar frontend with a low-profile, low-loss printed antenna," *IEEE Transactions on Microwave Theory and Techniques*, vol. 47, pp. 2237–2241, 1999.

[5] W. Menzel, D. Pilz, and M. Al-Tikriti, "MM-Wave folded reflector antennas with high gain, low loss, and low profile," *IEEE Antennas and Propagation Magazine*, pp. 24–29, 2002.

[6] A. Chakraborty, B. N. Das, and G. S. Sanyal, "Beam shaping using non-linear phase distribution in a uniformly spaced array," *IEEE Transactions on Antennas and Propagation*, vol. 30, pp. 1031–1034, 1982.